ATLAS NOTE

ATLAS-CONF-2013-054

May 14, 2013

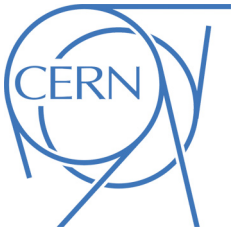

Search for new phenomena using final states with large jet multiplicities and missing transverse momentum with ATLAS in 20 fb^{-1} of $\sqrt{s}$ = 8 TeV proton-proton collisions

The ATLAS Collaboration

ATLAS-CONF-2013-054
16 May 2013

Abstract

A search is presented for new particles decaying to large numbers of jets in association with missing transverse momentum using 20.3 fb^{-1} of pp collision data at $\sqrt{s}$ = 8 TeV collected by the ATLAS experiment at the Large Hadron Collider. The event selection requires missing transverse momentum, no isolated electrons or muons, and from 7 to ≥10 jets. The sensitivity of the search is enhanced by considering the number of b-tagged jets and the scalar sum of masses of large-radius (R = 1.0) jets in an event. No evidence is found for physics beyond the Standard Model. The results are interpreted in the context of various simplified supersymmetry-inspired models, as well as a mSUGRA/CMSSM model with the lightest Higgs boson mass close to the mass of the recently observed boson.

1 Introduction

Many extensions of the Standard Model of particle physics predict the presence of TeV-scale strongly interacting particles that decay to lighter, weakly interacting descendants. Any such weakly interacting particles that are massive and stable can contribute to the dark matter content of the universe. The strongly interacting parents would be produced in the proton-proton interactions at the Large Hadron Collider (LHC) [1], and such events would be characterized by significant missing transverse momentum from the unobserved weakly interacting daughters, and jets from emissions of quarks and/or gluons.

In the context of R-parity conserving supersymmetry (SUSY) [2], the strongly interacting parent particles are the partners of the quarks (squarks, $\tilde{q}$) and the partners of the gluons (gluinos, $\tilde{g}$), and are produced in pairs. The lightest supersymmetric particle (LSP) is stable, providing a candidate that can contribute to the relic dark matter density in the universe [3].

If kinematically accessible, the squarks and gluinos are produced in the pp collisions at the LHC. They can be expected to decay in cascades, the nature of which depends on the mass hierarchy within the model. Individual cascade decays may include gluino decays to top squarks (stop), $\tilde{t}$,

$$\tilde{g} \;\rightarrow\; \tilde{t} + \bar{t} \tag{1a}$$

followed by the top squark decay to a top quark and a neutralino, $\tilde{\chi}_1^0$,

$$\tilde{t} \rightarrow t + \tilde{\chi}_1^0. \tag{1b}$$

Alternatively, if the top squark is heavier than the gluino, the three body decay,

$$\tilde{g} \;\rightarrow\; t + \bar{t} + \tilde{\chi}_1^0 \tag{2}$$

may result. Other possibilities include decays involving intermediate charginos, neutralinos, and/or squarks including bottom squarks. A pair of cascade decays will produce a large number of Standard Model particles, together with a pair of LSPs, one from the end of each cascade. The LSPs are assumed to be stable and weakly interacting, and so result in missing transverse momentum.

In this note we consider final states with large numbers of jets together with significant missing transverse momentum in the absence of isolated electrons or muons, using the pp collision data recorded by the ATLAS experiment during 2012 at a centre-of-mass energy of $\sqrt{s} = 8$ TeV. The corresponding integrated luminosity is 20.3 fb^{-1}. Searches for new phenomena in final states with large jet multiplicities – requiring from at least six to at least nine jets – and missing transverse momentum have previously been reported by the ATLAS collaboration using LHC pp collision data corresponding to 1.34 fb^{-1} [4] and to 4.7 fb^{-1} [5] at $\sqrt{s} = 7$ TeV. Searches with explicit tagging of jets from bottom quarks (b-jets) in multi-jet events were also performed by ATLAS [6] and CMS [7, 8, 9]. These searches found no significant excess over the Standard Model expectation and provided stringent limits on various supersymmetric models, including decays such as (2) and a mSUGRA/CMSSM [10] model that includes strong production processes. The analysis presented in this note extends previous analyses by reaching higher jet multiplicities and utilizing new sensitive variables.

Events are first selected with large jet multiplicities, with requirements ranging from at least seven to at least ten jets, reconstructed using the anti-k_t clustering algorithm [11] and jet distance parameter of $R = 0.4$. Significant missing transverse momentum is also required in the event. An additional selection based on the number of b-jets gives enhanced sensitivity to models which predict either more or fewer b-jets than the Standard Model background. In a complementary stream of the analysis, the $R = 0.4$ jets are re-clustered into large ($R = 1.0$) composite jets to form an event variable, the sum of the masses of the composite jets, which gives additional discrimination in models with a large number of objects in the final state [12]. Events containing isolated, high-p_{T} electrons or muons are vetoed in order to reduce

backgrounds involving leptonic W boson decays. Compared to the previous analyses [4, 5] those signal regions that had the smallest jet multiplicity are omitted as they are redundant by the already existing stringent limits on large cross-section models. Additionally the usage of b-jets and large composite jets is new and enhances the sensitivity of the search.

This search has been confirmed to have good sensitivity to decays such as (1) and (2) (see e.g. Ref. [5]), but it should also provide sensitivity to any model resulting in a final state with large jet multiplicity in association with missing transverse momentum. Such models include the pair production of gluinos, each of them decaying via:

$$\tilde{g} \rightarrow q + \tilde{q} \tag{3a}$$

followed by squark decay (with an intermediate chargino, $\tilde{\chi}_1^{\pm}$),

$$\tilde{q} \rightarrow q + W + \tilde{\chi}_1^0, \tag{3b}$$

or alternatively (with an intermediate $\tilde{\chi}_1^{\pm}$ and an intermediate neutralino, $\tilde{\chi}_2^0$),

$$\tilde{q} \rightarrow q + W + Z + \tilde{\chi}_1^0. \tag{3c}$$

Another possibility is the pair production of gluinos which decay as in (1a) and the subsequent decay of the $\tilde{t}$ via:

$$\tilde{t} \rightarrow b + \tilde{\chi}_1^{\pm} \tag{4}$$

or via the R-parity violating decay:

$$\tilde{t} \rightarrow b + s. \tag{5}$$

Several supersymmetry models are used to interpret the analysis results; models that include decays such as (1), (2) and (3); and a mSUGRA/CMSSM model with parameters[1] $\tan\beta = 30$, $A_0 = -2m_0$ and $\mu > 0$, which accommodates a lightest Higgs boson mass compatible with the observed Higgs boson mass at the LHC [13].

2 The ATLAS detector and data samples

The ATLAS experiment is a multi-purpose particle physics detector with a forward-backward symmetric cylindrical geometry and nearly 4π coverage in solid angle.[2] The layout of the detector is defined by four superconducting magnet systems, which comprise a thin solenoid surrounding inner tracking detectors (ID), and a barrel and two end-cap toroids surrounding a large muon spectrometer. The calorimeters lay between the ID and the muon system. In the pseudorapidity region $|\eta| < 3.2$, high-granularity liquid-argon (LAr) electromagnetic (EM) sampling calorimeters are used. An iron/scintillator-tile calorimeter provides hadronic coverage for $|\eta| < 1.7$. The end-cap and forward regions, spanning $1.5 < |\eta| < 4.9$, are instrumented with LAr calorimetry for both EM and hadronic measurements.

The data sample used in this analysis was taken during the period from March to December 2012 with the LHC operating at a pp centre-of-mass energy of $\sqrt{s} = 8$ TeV. Application of data-quality requirements results in a corresponding integrated luminosity of $20.3 \pm 0.6\,\text{fb}^{-1}$, where the luminosity is measured using similar techniques to those described in Ref. [14], with a preliminary calibration of

[1] A particular mSUGRA/CMSSM model point is specified by five parameters: the universal scalar mass m_0, the universal gaugino mass $m_{1/2}$, the universal trilinear scalar coupling A_0, the ratio of the vacuum expectation values of the two Higgs fields $\tan\beta$, and the sign of the higgsino mass parameter μ.

[2] ATLAS uses a right-handed coordinate system with its origin at the nominal interaction point in the centre of the detector and the z-axis along the beam pipe. Cylindrical coordinates (r, ϕ) are used in the transverse plane, ϕ being the azimuthal angle around the beam pipe. The pseudorapidity η is defined in terms of the polar angle θ by $\eta = -\ln\tan(\theta/2)$, and the transverse energy E_{T} by $E_{\text{T}} = E\sin\theta$.

the luminosity scale derived from beam-separation scans performed in November 2012. The analysis makes use of dedicated multi-jet triggers, the final step of which required either at least five jets with $E_{\mathrm{T}} > 55$ GeV or at least six jets with $E_{\mathrm{T}} > 45$ GeV, where the jets must have $|\eta| < 3.2$. The final level of online trigger selection is based on a jet algorithm and calibration method closely matched to those used in the offline selection. In all cases the trigger efficiency is greater than 99% for events satisfying the offline jet multiplicity selections of the signal regions described in Section 4. Single-lepton triggers and prescaled multi-jet triggers are used for background determination in control regions.

3 Object selection

Jets are reconstructed using the anti-k_t jet clustering algorithm with distance parameter of 0.4. The inputs to this algorithm are clusters of calorimeter cells seeded by cells with energy significantly above the noise level. Jet momenta are constructed by performing a four-vector sum over these clusters of calorimeter cells, treating each as an $(E, \mathbf{p})$ four-vector with zero mass. The local cluster weighting (LCW) calibration method [15] is used to classify clusters as either being of electromagnetic or hadronic origin and based on this classification applies specific energy corrections derived from a combination of Monte Carlo simulation and data. An additional calibration is subsequently applied to the corrected jet energies relating the response of the calorimeter to the true jet energy. The jets are corrected for energy from additional proton-proton collisions (pile-up) using a method, suggested in [16], which estimates the pile-up activity in any given event, as well as the sensitivity of any given jet to pile-up. The method subtracts a contribution from the jet energy equal to the product of the jet area and the event average energy density. Jets are required to satisfy $p_{\mathrm{T}} > 20$ GeV and $|\eta| < 2.8$. More stringent requirements on p_{T} and on $|\eta|$ are made when defining signal regions as described in Section 4.

Jets with heavy flavour content are identified using a tagging algorithm that uses both impact parameter and secondary vertex information [17]. Jets have the potential to be b-tagged provided that they satisfy both $|\eta| < 2.5$ and $p_{\mathrm{T}} > 40$ GeV. The parameters of the algorithm are chosen such that 70% of b-jets and about 1% of light flavour or gluon jets are selected in $t\bar{t}$ events in Monte Carlo simulations [18]. Jets initiated by charm quarks are tagged with about 20% efficiency.

Electrons are required to have $p_{\mathrm{T}} > 10$ GeV and $|\eta| < 2.47$. They must satisfy 'medium' electron shower shape and track selection criteria based upon those described in Ref. [19], but modified to reduce the impact of pile-up and to match tightened trigger requirements, and they must be separated by at least $\Delta R = 0.4$ from any jet, where $\Delta R = \sqrt{(\Delta\eta)^2 + (\Delta\phi)^2}$. Events containing electrons passing these criteria are vetoed when forming signal regions. Additional requirements are applied to electrons when defining leptonic control regions used to aid in the estimate of the SM background contributions; in this case, electrons must have $p_{\mathrm{T}} > 25$ GeV, must satisfy the 'tight' criteria, must have transverse and longitudinal impact parameters within 5σ and 0.4 mm, respectively, of the primary vertex, and are required to be well isolated.[3]

Muons are required to have $p_{\mathrm{T}} > 10$ GeV and $|\eta| < 2.5$, to satisfy track quality selection criteria, and to be separated by at least $\Delta R = 0.4$ from the nearest jet candidate. Events containing muons passing these criteria are vetoed when forming signal regions. When defining leptonic control regions muons must have $p_{\mathrm{T}} > 25$ GeV, $|\eta| < 2.4$, transverse and longitudinal impact parameters within 5σ and 0.4 mm, respectively, of the primary vertex and they must be isolated.[4]

[3]The electron isolation requirements are based on nearby tracks and calorimeter clusters, as follows. The scalar sum of transverse momenta of tracks other than the electron one in a cone of radius $\Delta R = 0.3$ around the electron is required to be smaller than 16% of the electron's p_{T}. The scalar sum of calorimeter transverse energy around the electron in the same cone is required to be smaller than 18% of the electron's p_{T}.

[4]The scalar sum of the transverse momenta of the tracks other than the muon one within a cone of $\Delta R = 0.3$ around the muon must be less than 12% of the muon's p_{T}, and the scalar sum of calorimeter transverse energy in the same cone (omitting

The missing transverse two-vector momentum $\mathbf{p}_{\mathrm{T}}^{\mathrm{miss}}$ is calculated from the negative vector sum of the transverse momenta of all calorimeter energy clusters and of all muons [20]. The magnitude of $\mathbf{p}_{\mathrm{T}}^{\mathrm{miss}}$, conventionally denoted $E_{\mathrm{T}}^{\mathrm{miss}}$, is used to distinguish signal and background regions in this analysis. Clusters associated with either electrons or photons with $p_{\mathrm{T}} > 10$ GeV, and those associated with jets with $p_{\mathrm{T}} > 20$ GeV make use of the calibrations of these respective objects. For jets the calibration includes the area-based pile-up correction described above. Clusters not associated with such objects are calibrated using both calorimeter and tracker information.

4 Event selection

Following the object reconstruction described in Section 3, events are discarded if they contain any jet failing quality criteria designed to suppress detector noise and non-collision backgrounds, or if they lack a reconstructed primary vertex with five or more associated tracks. Events containing electron or muon candidates are also vetoed. The remaining events are then analysed in two complementary analysis streams, both of which require large jet multiplicities and significant $E_{\mathrm{T}}^{\mathrm{miss}}$. The selections are verified to have good sensitivity to decays such as (1) and (2), but are maintained generic to ensure sensitivity in a broad set of models with large jet multiplicity and $E_{\mathrm{T}}^{\mathrm{miss}}$ in the final state.

4.1 The multi-jet + flavour stream

In the multi-jet + flavour stream the number of jets with $|\eta| < 2$ and p_{T} above the threshold $p_{\mathrm{T}}^{\mathrm{min}} = 50$ GeV is calculated. Events with exactly eight jets or exactly nine jets are selected, and are further subdivided according to the number of the jets (0, 1 or ≥2) with $p_{\mathrm{T}} > 40$ GeV and $|\eta| < 2.5$ which satisfy the b-tagging requirements. Events with ten or more jets are retained in a separate category, without any further subdivision.

A similar process is performed for the higher jet p_{T} threshold of $p_{\mathrm{T}}^{\mathrm{min}} = 80$ GeV. Signal regions are defined for events with exactly seven jets or at least eight jets. Both categories are again subdivided according to the number of jets (0, 1 or ≥2) with $p_{\mathrm{T}} > 40$ GeV which are b-tagged. For each value of $p_{\mathrm{T}}^{\mathrm{min}}$, the b-tagged jets may belong to the set of jets with p_{T} greater than $p_{\mathrm{T}}^{\mathrm{min}}$, but this is not a requirement.

In all cases the final selection variable is $E_{\mathrm{T}}^{\mathrm{miss}}/\sqrt{H_{\mathrm{T}}}$, the ratio of the $E_{\mathrm{T}}^{\mathrm{miss}}$ to the square root of the scalar sum H_{T} of the transverse momenta of all jets with $p_{\mathrm{T}} > 40$ GeV and $|\eta| < 2.8$. This ratio is closely related to the significance of the $E_{\mathrm{T}}^{\mathrm{miss}}$ relative to the resolution due to stochastic variations in the measured jet energies [20]. The value of $E_{\mathrm{T}}^{\mathrm{miss}}/\sqrt{H_{\mathrm{T}}}$ is required to be larger than 4 $\mathrm{GeV}^{1/2}$ for all signal regions.

4.2 The multi-jet + M_J^{Σ} stream

The multi-jet + M_J^{Σ} stream proceeds as follows. The number of ($R = 0.4$) jets with p_{T} above 50 GeV is determined, this time using a larger pseudorapidity acceptance of $|\eta| < 2.8$. Events with at least eight, at least nine or at least ten such jets are retained, and a category is created for each of those multiplicity thresholds. The four-vectors of the $R = 0.4$ jets satisfying $p_{\mathrm{T}} > 20$ GeV and $|\eta| < 2.8$ are then used as inputs to a second iteration of the anti-k_t jet algorithm, this time using the larger distance parameter of $R = 1.0$. The resulting larger objects are denoted *composite jets*. The selection variable M_J^{Σ} is then defined to be the sum of the masses $m_j^{R=1.0}$ of the composite jets

$$M_J^{\Sigma} \equiv \sum_j m_j^{R=1.0}, \tag{6}$$

that from the muon itself) must be less than 12% of the muon's p_{T}.

	Multi-jet + flavour stream												**Multi-jet + M_J^Σ stream**		
Identifier	**8j50**			**9j50**			**≥ 10j50**	**7j80**			**≥ 8j80**			**≥ 8j50**	**≥ 9j50**	**≥ 10j50**
Jet $\lvert\eta\rvert$	< 2.0							< 2.0						< 2.8		
Jet p_{T}	$> 50\,\mathrm{GeV}$							$> 80\,\mathrm{GeV}$						$> 50\,\mathrm{GeV}$		
Jet count	$= 8$			$= 9$			≥ 10	$= 7$			≥ 8			≥ 8	≥ 9	≥ 10
b-jets ($p_{\mathrm{T}} > 40$ GeV, $\lvert\eta\rvert < 2.5$)	0	1	≥ 2	0	1	≥ 2	—	0	1	≥ 2	0	1	≥ 2	—		
M_J^Σ [GeV]	—							—						> 340 and > 420 for each case		
$E_{\mathrm{T}}^{\mathrm{miss}} / \sqrt{H_{\mathrm{T}}}$	$> 4\,\mathrm{GeV}^{1/2}$							$> 4\,\mathrm{GeV}^{1/2}$						$> 4\,\mathrm{GeV}^{1/2}$		

Table 1: Definition of the signal regions. The jet $\lvert\eta\rvert$, p_{T} and multiplicity all refer to the $R = 0.4$ jets. Larger distance parameter ($R = 1.0$) composite jets are used in the multi-jet + M_J^Σ stream when constructing M_J^Σ. A long dash '—' indicates that no requirement is made.

where the sum is over those composite jets which satisfy $p_{\mathrm{T}}^{R=1.0} > 100$ GeV and $|\eta^{R=1.0}| < 1.5$. Signal regions are defined for two different M_J^{Σ} thresholds. Again the final selection requires that $E_{\mathrm{T}}^{\mathrm{miss}} / \sqrt{H_{\mathrm{T}}} > 4$ GeV$^{1/2}$.

4.3 Summary of signal regions

The nineteen resulting signal regions are shown in Table 1. Within the multi-jet + flavour stream the seven signal regions defined with $p_{\mathrm{T}}^{\mathrm{min}} = 50$ GeV are mutually disjoint. The same is true for the six signal regions defined with the threshold of 80 GeV. However, the two sets of signal regions overlap; an event found in one of the $p_{\mathrm{T}}^{\mathrm{min}} = 80$ GeV signal regions may also be found in one of the $p_{\mathrm{T}}^{\mathrm{min}} = 50$ GeV signal regions. The multi-jet + M_J^{Σ} stream has six inclusive signal regions; for example an event which has at least ten $R = 0.4$ jets with $p_{\mathrm{T}} > 50$ GeV, $M_J^{\Sigma} > 420$ GeV and $E_{\mathrm{T}}^{\mathrm{miss}} / \sqrt{H_{\mathrm{T}}} > 4$ GeV$^{1/2}$ will be found in all six multi-jet + M_J^{Σ} regions. These overlaps are treated in the analysis results as described in Section 6.

5 Background determination

The dominant backgrounds are multi-jet production, including purely strong interaction processes and fully hadronic decays of $t\bar{t}$, and hadronic decays of W and Z bosons in association with jets; semi- and fully-leptonic decays of $t\bar{t}$; and leptonically decaying W or Z bosons produced in association with jets. Non-fully-hadronic $t\bar{t}$, and events with leptonic decays of W and Z bosons are collectively referred to as leptonic backgrounds.

The major backgrounds (multi-jet, $t\bar{t}$, W + jets, and Z + jets) are determined with the aid of control regions, which are defined such that they are enriched in the background process(es) of interest, but nevertheless remain kinematically close to the signal regions. The multi-jet background determination is fully data-driven, and the most significant of the other backgrounds use data control regions to normalize simulations. The normalizations of the simulations are adjusted simultaneously in all the control regions using a binned fit described in Section 6, and the simulation is used to extrapolate the results into the signal regions. The methods used in the determination of the multi-jet and leptonic backgrounds are described in Sections 5.2 and 5.4, respectively.

5.1 Monte Carlo simulations

Monte Carlo simulations are used as part of the leptonic background determination process, and to assess the sensitivity to specific SUSY signal models. Most of the leptonic backgrounds are generated using Sherpa-1.4.1 [21] with the PDF set CT10 [22]. For $t\bar{t}$ production, up to four additional partons are modelled in the matrix element. W + jets and Z + jets are generated with up to five additional partons in the matrix element, except for processes involving b-quarks for which up to four additional partons are included in the matrix element. In all cases, additional jets are generated via parton showering. The leptonic W + jets, Z + jets and $t\bar{t}$ backgrounds are normalized according to their inclusive theoretical cross sections [23]. In the case of $t\bar{t}$ production, the agreement with data in the validation regions is improved by reweighting the relative fraction of gluon-gluon initiated events to other processes. The estimation of the leptonic backgrounds in the signal regions is described in detail in Section 5.4.

Smaller background contributions are also modelled for the following processes: single top quark production in association with a W boson and in the s-channel (MC@NLO 4.06 [24] / Herwig 6.520 [25] / Jimmy 4.31 [26]), t-channel single top quark production (AcerMC3.8 [27] / Pythia-6.426 [28]), and $t\bar{t}$ production in association with a W or Z boson (Madgraph-5.1.4.8 [29] / Pythia-6.426).

Supersymmetric production processes are generated using Herwig++2.5.2 [30] and Madgraph-5.1.4.8 with the PDF set CTEQ6L1 [31]. The cross sections are calculated to next-to-leading order in the strong

coupling constant α_S, including the resummation of soft gluon emission at next-to-leading-logarithmic accuracy (NLO+NLL) [32].

For each process, the nominal cross section and the uncertainty is taken from an envelope of cross section predictions using different PDF sets and factorisation and renormalization scales, as described in Ref. [33]. All Monte Carlo samples also include simulation of pile-up and employ a detector simulation [34] based on `GEANT4` [35]. The are also reconstructed with the same algorithms as the data.

5.2 Multi-jet backgrounds

The dominant background at intermediate values of $E_{\mathrm{T}}^{\mathrm{miss}}$ is multi-jet production including purely strong interaction processes and fully hadronic decays of $t\bar{t}$. The contribution from these processes is determined using collision data and the selection criteria have been designed such that multi-jet processes can be accurately determined from supporting measurements.

The method [4, 5] is based on the observation that the $E_{\mathrm{T}}^{\mathrm{miss}}$ resolution of the detector is approximately proportional to $\sqrt{H_{\mathrm{T}}}$ and almost independent of the jet multiplicity in events dominated by jet activity, including hadronic decays of top quarks and gauge bosons. The distribution of the ratio $E_{\mathrm{T}}^{\mathrm{miss}}/\sqrt{H_{\mathrm{T}}}$ therefore has a shape that is almost invariant under changes in the jet multiplicity. The multi-jet backgrounds therefore can be determined using control regions with lower $E_{\mathrm{T}}^{\mathrm{miss}}/\sqrt{H_{\mathrm{T}}}$ and/or lower jet multiplicity than the signal regions.

Events containing heavy quarks show a different $E_{\mathrm{T}}^{\mathrm{miss}}/\sqrt{H_{\mathrm{T}}}$ distribution than those containing only light-quark or gluon jets, since semileptonic decays of heavy quarks contain neutrinos. The dependence of $E_{\mathrm{T}}^{\mathrm{miss}}/\sqrt{H_{\mathrm{T}}}$ on the number of heavy quarks is accounted for in the multi-jet + flavour signal regions by using a consistent set of such control regions with the same b-jet multiplicity as the target signal distribution. The $E_{\mathrm{T}}^{\mathrm{miss}}/\sqrt{H_{\mathrm{T}}}$ distribution is also found to be approximately independent of the M_J^{Σ} event shape variable, so a similar technique is used to obtain the expected multi-jet background contributions to the multi-jet + M_J^{Σ} signal regions.

The leading source of variation in $E_{\mathrm{T}}^{\mathrm{miss}}/\sqrt{H_{\mathrm{T}}}$ to changes in the jet multiplicity comes from a contribution to $E_{\mathrm{T}}^{\mathrm{miss}}$ from calorimeter energy deposits not associated to jets and hence not contributing to H_{T}. The effect of this 'soft' energy is corrected for by reweighting the $E_{\mathrm{T}}^{\mathrm{miss}}/\sqrt{H_{\mathrm{T}}}$ distribution separately for each SR jet multiplicity, to provide the same $\sum \mathrm{E}_{\mathrm{T}}^{\mathrm{CellOut}}/H_{\mathrm{T}}$ distribution, where $\sum \mathrm{E}_{\mathrm{T}}^{\mathrm{CellOut}}$ is the scalar sum of E_{T} over all clusters of calorimeter cells not associated with jets having $p_{\mathrm{T}} > 20$ GeV or electron, or muon candidates.

For example, to obtain the multi-jet contribution to the multi-jet + flavour stream 9j50 signal region, with exactly one b-jet the procedure is as follows. A template of the shape of the $E_{\mathrm{T}}^{\mathrm{miss}}/\sqrt{H_{\mathrm{T}}}$ distribution is formed from events with exactly six jets with $p_{\mathrm{T}} > 50\,\mathrm{GeV}$, and with exactly one b-jet. The events are weighted so that they have the same normalized $\sum \mathrm{E}_{\mathrm{T}}^{\mathrm{CellOut}}/H_{\mathrm{T}}$ distribution in the region $E_{\mathrm{T}}^{\mathrm{miss}}/\sqrt{H_{\mathrm{T}}} < 1.5\ \mathrm{GeV}^{1/2}$ as is found in the nine-jet region satisfying the same $E_{\mathrm{T}}^{\mathrm{miss}}/\sqrt{H_{\mathrm{T}}}$ and b-jet criteria. The expected contribution from leptonic backgrounds is then subtracted, so that the template provides the expected distribution resulting from the detector resolution, together with any contribution to the resolution from leptonic b decays. The nine-jet prediction for the signal region ($E_{\mathrm{T}}^{\mathrm{miss}}/\sqrt{H_{\mathrm{T}}} > 4\ \mathrm{GeV}^{1/2}$) with exactly one b-jet is then given by

$$N_{\text{predicted}}^{\text{SR, multi-jet}} = \left(N_{\text{data}}^{A,\, n^{\text{jet}}=9} - N_{\text{leptonic MC}}^{A,\, n^{\text{jet}}=9}\right) \times \left(\frac{N_{\text{data}}^{B,\, n^{\text{jet}}=6} - N_{\text{leptonic MC}}^{B,\, n^{\text{jet}}=6}}{N_{\text{data}}^{A,\, n^{\text{jet}}=6} - N_{\text{leptonic MC}}^{A,\, n^{\text{jet}}=6}}\right),$$

where $A \equiv E_{\mathrm{T}}^{\mathrm{miss}}/\sqrt{H_{\mathrm{T}}} < 1.5\ \mathrm{GeV}^{1/2}$, $B \equiv E_{\mathrm{T}}^{\mathrm{miss}}/\sqrt{H_{\mathrm{T}}} > 4\ \mathrm{GeV}^{1/2}$, and each of the counts N are made after requiring the same b-jet multiplicity as for the target signal region (i.e. exactly one b-jet in this example). As has already been noted, the six jet region counts are weighted to provide the same $\sum \mathrm{E}_{\mathrm{T}}^{\mathrm{CellOut}}/H_{\mathrm{T}}$ distribution as the nine jet region.

An analogous procedure is used to obtain the expected multi-jet contribution to each of the other multi-jet + flavour stream signal regions by using the appropriate $p_{\mathrm{T}}^{\mathrm{min}}$, jet multiplicity, and b-jet multiplicity as required by the target signal region. In each case the shape of the $E_{\mathrm{T}}^{\mathrm{miss}}/\sqrt{H_{\mathrm{T}}}$ distribution is obtained from a 'template' with exactly six (five) jets for signal regions with $p_{\mathrm{T}}^{\mathrm{min}} = 50\,(80)$ GeV. The distribution of $E_{\mathrm{T}}^{\mathrm{miss}}/\sqrt{H_{\mathrm{T}}}$ for multi-jet + flavour stream control regions are shown in Fig. 1.

The procedure in the multi-jet + M_J^{Σ} stream is similar: the same jet $p_{\mathrm{T}}^{\mathrm{min}}$, jet multiplicity and M_J^{Σ} criteria are used when forming the template and control regions that are required for the target signal region. $E_{\mathrm{T}}^{\mathrm{miss}}/\sqrt{H_{\mathrm{T}}}$ distributions for control regions with exactly seven jets with p_{T}>50 GeV and additional M_J^{Σ} selections are shown in Fig. 2. Leptonic backgrounds are subtracted, and $\sum \mathrm{E}_{\mathrm{T}}^{\mathrm{CellOut}}/H_{\mathrm{T}}$ weighting is applied. In each case the $E_{\mathrm{T}}^{\mathrm{miss}}/\sqrt{H_{\mathrm{T}}}$ template shape is determined from a sample which has exactly six jets with $p_{\mathrm{T}} > 50$ GeV.

Variations in the shape of the $E_{\mathrm{T}}^{\mathrm{miss}}/\sqrt{H_{\mathrm{T}}}$ are later used to quantify the systematic uncertainty associated with the method, as described in Section 5.3.

5.3 Systematic uncertainties in the multi-jet background determination

The multi-jet background determination method is validated by measuring the accuracy of predictions for regions with jet multiplicities and/or $E_{\mathrm{T}}^{\mathrm{miss}}/\sqrt{H_{\mathrm{T}}}$ smaller than those chosen for the signal regions. The consistency of the prediction with the number of observed events (*closure*) is tested in regions with $E_{\mathrm{T}}^{\mathrm{miss}}/\sqrt{H_{\mathrm{T}}}$ [$\mathrm{GeV}^{1/2}$] in the ranges (1.5, 2.0), (2.0, 2.5), and (2.5, 3.5) for jet multiplicities of exactly seven, eight and nine, and in the range (1.5, 2.0) and (2.0, 3.5) for ≥10 jets. The tests are performed separately for 0, 1 and ≥ 2 b-tagged jets. In addition, the method is tested for events with exactly six (five) jets with $p_{\mathrm{T}}^{\mathrm{min}} = 50$ GeV (80 GeV) across the full range of $E_{\mathrm{T}}^{\mathrm{miss}}/\sqrt{H_{\mathrm{T}}}$ in this case using a template obtained from events with exactly five (four) jets. The five-jet (four-jet) events are obtained using a prescaled trigger for which only a fraction of the total luminosity is available. Agreement is found both for signal region jet multiplicities at intermediate values of $E_{\mathrm{T}}^{\mathrm{miss}}/\sqrt{H_{\mathrm{T}}}$ and also for the signal region $E_{\mathrm{T}}^{\mathrm{miss}}/\sqrt{H_{\mathrm{T}}}$ selection at lower multiplicity. A symmetrical systematic uncertainty on any signal region is constructed by the maximal deviation in any of the closure regions with the same jet multiplicity or lower, for the same b-tagging requirements. Typical closure uncertainties are mostly in the range 5% to 15%; they can grow as large as ∼50% for the tightest signal regions, due to larger statistical variations in the corresponding control regions.

Additional systematic uncertainties result from modeling of the heavy flavour content (25%), which is assessed by using combinations of the templates of different b-tagged jet multiplicity to vary the purity of the different samples. The closure in simulation of samples with high heavy flavour content is also tested. The leptonic backgrounds that are subtracted when forming the template have an uncertainty associated with it (5-20%, depending on the signal region). Furthermore, uncertainties are accounted for due to the scale choice of the cutoff for the soft energy term, $\sum \mathrm{E}_{\mathrm{T}}^{\mathrm{CellOut}}$, (3-15%) and the trigger efficiency (<1%) in the region where the template is formed.

5.4 Leptonic backgrounds

The leptonic backgrounds are defined to be those which involve the leptonic decays $W \to \ell\nu$ or $Z \to \nu\nu$. Contributions are determined for non-fully-hadronic (i.e. semi-leptonic or di-leptonic) $t\bar{t}$, single top, W and Z production, and di-boson production, each in association with jets. The category excludes semi-leptonic decays of heavy flavour quarks which are considered within the multi-jet category (Section 5.2).

The leptonic backgrounds which contribute most to the signal regions are $t\bar{t}$ and W + jets. In each case events can evade the lepton veto either via hadronic τ decays or when electrons or muons are produced but not reconstructed. The predictions employ the Monte Carlo simulations described in Section 5.1. When predictions are taken directly from the Monte Carlo, the leptonic background event yields are

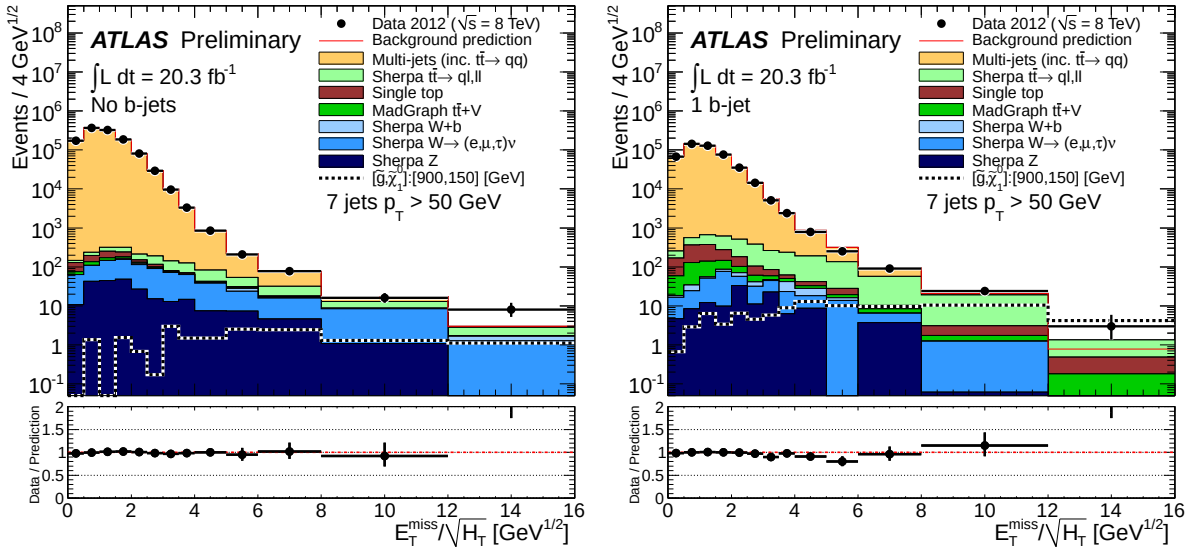

(a) No b-jets

(b) Exactly one b-jet

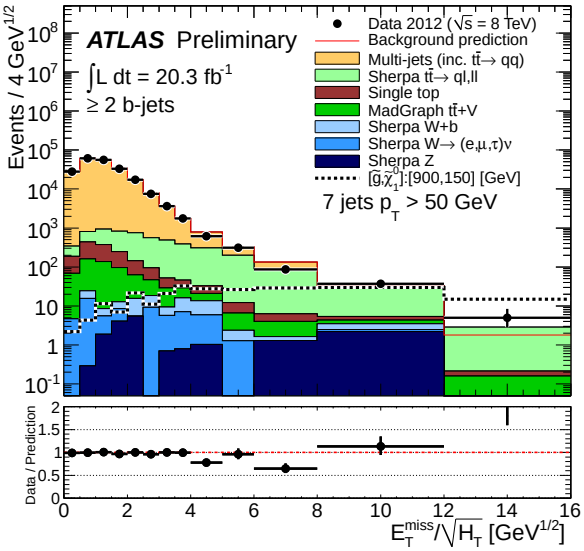

(c) At least two b-jets

Figure 1: Distribution of $E_{\mathrm{T}}^{\mathrm{miss}}/\sqrt{H_{\mathrm{T}}}$ for the control regions with exactly seven jets with $p_{\mathrm{T}} \geq 50$ GeV and $|\eta| < 2.0$, for different b-jet multiplicities. The multi-jet prediction is determined from a $E_{\mathrm{T}}^{\mathrm{miss}}/\sqrt{H_{\mathrm{T}}}$ template obtained from events with exactly six jets. It is normalized to the data in the region $E_{\mathrm{T}}^{\mathrm{miss}}/\sqrt{H_{\mathrm{T}}} < 1.5$ GeV$^{1/2}$ after subtraction of the leptonic backgrounds. The most important leptonic backgrounds are also shown, based on Monte Carlo simulations. Variable bin sizes are used with bin widths (in units of GeV$^{1/2}$) of 0.5 (up to $E_{\mathrm{T}}^{\mathrm{miss}}/\sqrt{H_{\mathrm{T}}} = 4$ GeV$^{1/2}$), 1 (from 4 to 6), 2 (from 6 to 8) and 4 thereafter. For reference and comparison, a supersymmetric model is used where gluinos of mass 900 GeV are pair produced and each decay as in (2) to two top quarks and a $\tilde{\chi}_1^0$ with a mass of 150 GeV. The model is referred to as '$[\tilde{g},\tilde{\chi}_1^0]$: [900, 150] [GeV]'.

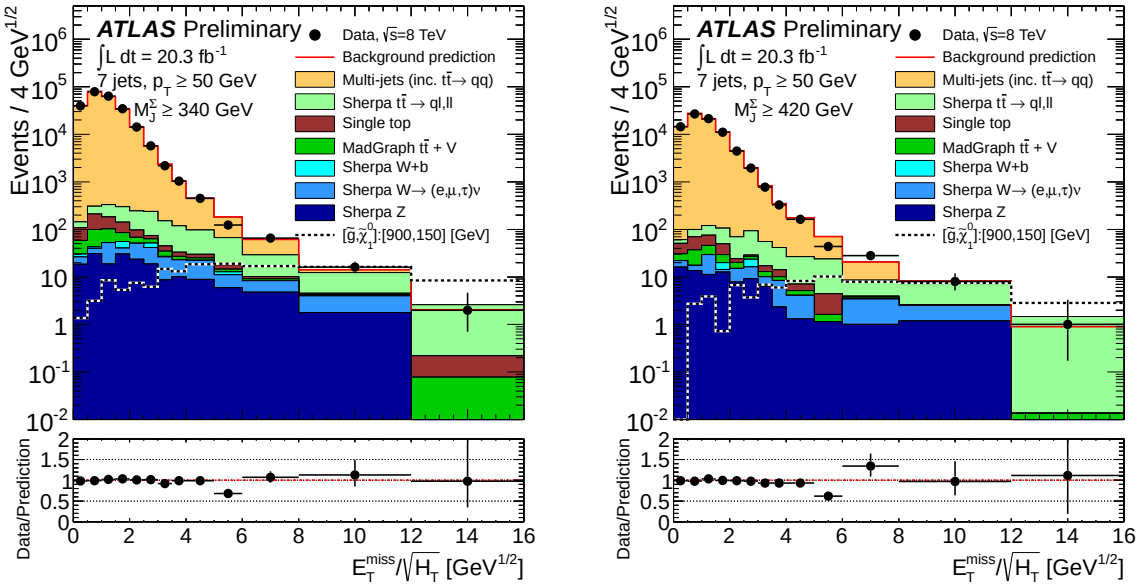

(a) $M_J^\Sigma \geq 340$ GeV (b) $M_J^\Sigma \geq 420$ GeV

Figure 2: Distribution of $E_{\mathrm{T}}^{\mathrm{miss}}/\sqrt{H_{\mathrm{T}}}$ for control regions with exactly seven jets with $p_{\mathrm{T}} \geq 50$ GeV, and satisfying the same M_J^Σ requirements as the multi-jet + M_J^Σ stream signal regions. The multi-jet prediction was determined from a $E_{\mathrm{T}}^{\mathrm{miss}}/\sqrt{H_{\mathrm{T}}}$ template obtained from events with exactly six jets. Other details as for Fig. 1.

subject to theoretical uncertainties (30-90%, depending on the signal region) associated with the use of a leading-order Monte Carlo generator, including scale variations as well as varying the number of partons present in the matrix element calculation.

To reduce uncertainties from higher-order corrections and from Monte Carlo modeling and detector response, background predictions are, where possible, normalized to data using control regions and cross-checked against data in other validation regions. These control regions and validation regions are designed to be distinct from, but kinematically close to, the signal regions, and orthogonal to them by requiring an identified lepton candidate.

The validation and control regions for the $t\bar{t}$ and W + jets backgrounds are defined in Table 2. In single-lepton regions, a single lepton (e or μ) is required, with sufficient p_{T} to allow the leptonic trigger to be employed. Modest requirements on $E_{\mathrm{T}}^{\mathrm{miss}}$ and $E_{\mathrm{T}}^{\mathrm{miss}}/\sqrt{H_{\mathrm{T}}}$ reduce the background from fake leptons. An upper limit on

$$m_{\mathrm{T}} = \sqrt{2\left(|\mathbf{p}_{\mathrm{T}}^{\mathrm{miss}}||\mathbf{p}_{\mathrm{T}}^{\ell}| - \mathbf{p}_{\mathrm{T}}^{\mathrm{miss}} \cdot \mathbf{p}_{\mathrm{T}}^{\ell}\right)},$$

where $\mathbf{p}_{\mathrm{T}}^{\ell}$ is the transverse momentum vector of the lepton, decreases possible contamination from non-Standard-Model processes.

Since it is dominantly through hadronic τ decays that W and $t\bar{t}$ contribute to the signal regions, the corresponding control regions are created by recasting the muon or electron as a jet. If the electron or muon has sufficient p_{T} (without any additional calibration), it is considered as an additional 'jet' and it can contribute to the jet multiplicity count, and to H_{T} and hence to the selection variable $E_{\mathrm{T}}^{\mathrm{miss}}/\sqrt{H_{\mathrm{T}}}$. The same jet multiplicity as the signal region is required for the equivalent control regions. Additionally, the same criteria on $E_{\mathrm{T}}^{\mathrm{miss}}/\sqrt{H_{\mathrm{T}}}$, M_J^Σ and the number of b-tagged jets are required. For the M_J^Σ stream these control regions are further split into regions with no b-tagged jets and those with b-tagged jets to allow separation of contributions from W+jets and $t\bar{t}$. Provided the expected number of Standard Model

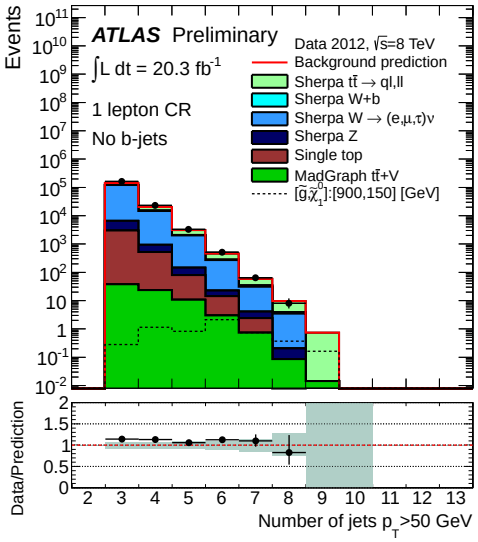

(a) No b-jets

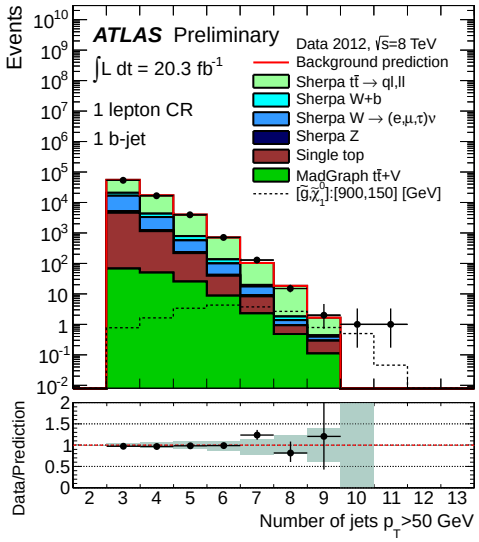

(b) Exactly one b-jet

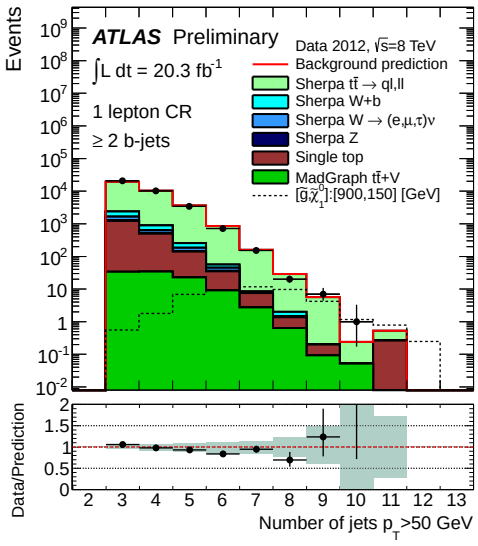

(c) $\geq$2 b-jets

Figure 3: Jet multiplicity distributions for $p_{\mathrm{T}}^{\mathrm{min}}$=50 GeV jets in the one-lepton $t\bar{t}$ and W + jets control regions (CR) for different b-jet multiplicities. Monte Carlo predictions are before fitting to data. Other details as for Fig. 1. The teal band in the ratio plot indicates the experimental uncertainties on the Monte Carlo prediction and also includes the Monte Carlo statistical uncertainty. Additional theoretical uncertainties are not shown.

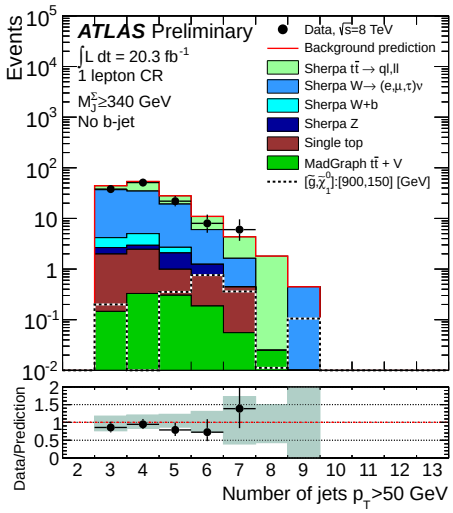

(a) M_J^{Σ}>340 GeV, no b-jets

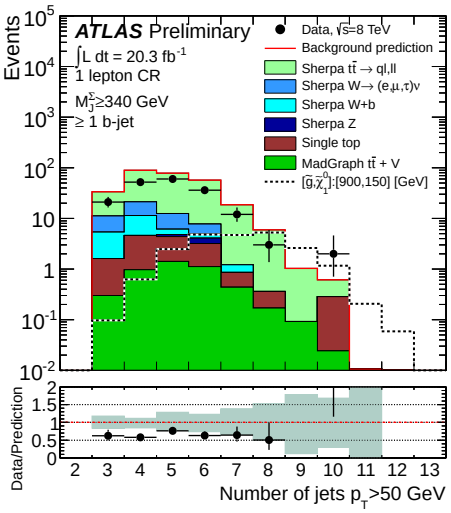

(b) M_J^{Σ}>340 GeV, ≥1 b-jets

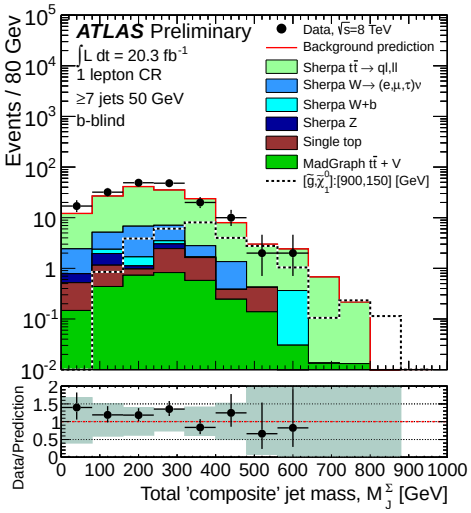

(c) M_J^{Σ} distribution, ≥7j50 selection applied

Figure 4: Jet multiplicity distributions for $p_{\mathrm{T}}^{\mathrm{min}} = 50$ GeV jets in the one-lepton $t\bar{t}$ and W + jets control regions (CR) for different b-jet multiplicities and a selection on $M_J^{\Sigma} > 340$ GeV (4a) - (4b), and the M_J^{Σ} distribution for an inclusive selection of seven jets with $p_{\mathrm{T}}^{\mathrm{min}} = 50$ GeV (4c). Other details as for Fig. 3.

Single lepton validation region	
Lepton p_{T}	$> 25\,\mathrm{GeV}$
Lepton multiplicity	Exactly one, $\ell \in \{e, \mu\}$
$E_{\mathrm{T}}^{\mathrm{miss}}$	$> 30\,\mathrm{GeV}$
$E_{\mathrm{T}}^{\mathrm{miss}} / \sqrt{H_{\mathrm{T}}}$	$> 2.0\ \mathrm{GeV}^{1/2}$
m_{T}	$< 120\,\mathrm{GeV}$
Jet p_{T}	As for signal regions (Table 1)
Jet multiplicity	
b-jet multiplicity	
M_J^{Σ}	
Control region (additional criteria)	
Jet multiplicity	Unit increment if $p_T^{\ell} > p_{\mathrm{T}}^{\mathrm{min}}$
$E_{\mathrm{T}}^{\mathrm{miss}} / \sqrt{H_{\mathrm{T}}\ (+p_{\mathrm{T}}^{\ell})}$	$> 4.0\ \mathrm{GeV}^{1/2}$

Table 2: The selection criteria for the validation and control regions for the $t\bar{t}$ and W + jets backgrounds. In the control region the lepton is recast as a jet so it contributes to H_{T} if $p_{\mathrm{T}}^{\ell} > 40\,\mathrm{GeV}$ and to the jet multiplicity count if $p_{\mathrm{T}}^{\ell} > p_{\mathrm{T}}^{\mathrm{min}}$.

events in the corresponding control region is greater than two, the number of observed events in that control region is used in a fit to determine the Standard Model background as described in Section 6. Distributions of jet multiplicity for the leptonic control regions can be found in Figures 3-4. In Figure 4 the M_J^{Σ} distribution for a leptonic control region is also shown.

The Z control regions require two same flavour leptons with an invariant mass consistent with that of the Z boson. To create control regions that emulate the signal regions, the lepton transverse momenta are added to the missing momentum two-vector and then the requirement $E_{\mathrm{T}}^{\mathrm{miss}} / \sqrt{H_{\mathrm{T}}} > 4\ \mathrm{GeV}^{1/2}$ is applied. This emulates the situation expected for the $Z \to \nu\nu$ background. The details of the selection are given in Table 3. This selection but with relaxed criteria is used to validate the Monte Carlo description of this process; however, insufficient events remain at high jet multiplicity, so the estimation of this background is taken from Monte Carlo simulations.

Two-lepton validation region	
Lepton p_{T}	$> 25\,\mathrm{GeV}$
Lepton multiplicity	Exactly two, e^+e^- or $\mu^+\mu^-$
$m_{\ell\ell}$	80 GeV to 100 GeV
Jet p_{T}	As for signal regions (Table 1)
Jet multiplicity	
b-jet multiplicity	
M_J^{Σ}	
Control region (additional criteria)	
$\lvert\mathbf{p}_{\mathrm{T}}^{\mathrm{miss}} + \mathbf{p}_{\mathrm{T}}^{\ell_1} + \mathbf{p}_{\mathrm{T}}^{\ell_2}\rvert / \sqrt{H_{\mathrm{T}}}$	$> 4.0\ \mathrm{GeV}^{1/2}$

Table 3: The selection criteria for the validation and control regions for the Z + jets background.

5.5 Systematic uncertainties in the leptonic background determination

Systematics on the leptonic backgrounds originate from both detector related and theoretical sources from the Monte Carlo modeling. Experimental uncertainties are dominated by those on jet energy scale and jet energy resolution. The ATLAS jet energy scale is determined using in-situ techniques and includes additional uncertainties associated with the quark-gluon composition of the sample, the heavy flavour fraction and pile-up uncertainties. The uncertainties are derived for $R = 0.4$ jets and propagated to all objects and selections used in the analysis. The various sources of the jet energy scale uncertainty are treated as correlated between the different Standard Model backgrounds as well as with the signal contributions when setting exclusion limits.

For the $t\bar{t}$ background, theoretical systematics are evaluated by comparing the predictions at particle level of the nominal SHERPA samples with additional samples in which some of the parameter settings have been varied. These include variations of the factorisation scale, the matching scale of the matrix element to the parton shower, the number of partons in the matrix element and the PDFs. ALPGEN [36] samples are also generated with the renormalization scale associated with α_S in the matrix element calculation varied up and down by a factor of two relative to the original scale k_T between two partons. Finally, samples with and without the relative weight of gluon-gluon initiated events to other processes are used to provide a systematic on this procedure.

Alternative samples are generated similarly for the other smaller backgrounds with different parameters and/or generators to assess the associated theoretical uncertainties.

6 Results

Figures 5-7 show the $E_T^{miss}/\sqrt{H_T}$ distributions for all the signal regions of both analysis streams. In order to check the consistency of the data with the background-only and the signal hypotheses, a simultaneous maximum likelihood fit is performed in the control and signal regions, for each of the analysis streams separately. A control region is taken into account in the fit if there are at least two expected events associated to it. The fits differ significantly between the two analysis streams, as described in what follows.

When evaluating a supersymmetric signal model for exclusion, any signal contamination in the control regions is taken into account for each signal point, as the control region fits are performed for each signal hypothesis. Separately, each signal region (one at a time), along with all control regions, is also fit under the background-only hypothesis. This fit is used to characterise agreement in each signal region with the background-only hypothesis, and to extract model-independent cross-section limits and upper limits on the production of events from new physics. For these model independent limits possible signal contamination in the control regions is neglected.

6.1 Simultaneous fit in the multi-jet + flavour stream

The seven $p_T^{min} = 50$ GeV signal regions (and similarly the six $p_T^{min} = 80$ GeV signal regions) are fit to the background and signal predictions. Correlations from sample to sample and region to region, separately for the $p_T^{min} = 50$ GeV and $p_T^{min} = 80$ GeV signal regions, are taken into account. Systematic uncertainties arising from the same source are treated as fully correlated.

The fit considers several independent background components:

- $t\bar{t}$ and W + jets. One control region is defined for each signal region, as described in Table 2; the normalization of each background component is allowed to vary freely in the fit.

- Less significant backgrounds (Z + jets, $t\bar{t} + W$, $t\bar{t} + Z$, and single top) determined using Monte Carlo simulations. These are individually allowed to vary within their uncertainties.

- Multi-jet background. Being data driven, it is not constrained in the fit by any control region. It is constrained in the signal regions with its uncertainties, which are described in Section 5.3.

The systematic effects, described in Sections 5.3 and 5.5, are treated as nuisance parameters in the fit. For the signal, the systematic effects included in the fit are the jet energy scale and resolution uncertainties, the b-tagging uncertainties, and the theoretical uncertainties.

6.2 Simultaneous fit in the multi-jet + M_J^Σ stream

Because the six multi-jet + M_J^Σ signal regions are inclusive, a simultaneous fit across control and signal regions would be difficult. Fits are only performed on a single signal-region basis to adjust the normalization of the $t\bar{t}$ and W + jets backgrounds using control regions, as defined in Table 2.

The systematic uncertainties affecting the background and signal predictions are treated as nuisance parameters in the fit. The following sources of uncertainty are considered: the jet energy scale, the jet energy resolution, and the theoretical uncertainties.

6.3 Fit results

Tables 4-7 summarize the fit results; the number of events observed in each of the signal regions, as well as their Standard Model background expectations, are reported before and after the fit to the control regions. In each of the signal regions, agreement is found between the Standard Model prediction and the data. The fit results are checked for stability and consistency with the background modelling based on the predictions described in Sections 5.2 and 5.4. There is no indication of a systematic mis-modelling of any of the major backgrounds; the fitted values are in all cases consistent to the Monte Carlo predictions.

In addition to the event yields, the probability (p_0-value) that a background-only pseudo-experiment is more signal-like than observed is given for each individual signal region. To obtain these p_0-values, the fit in the signal region proceeds in the same way as the control-region-only fit, except that the number of events observed in the signal region is included as an input to the fit. Then, an additional parameter for the non-Standard-Model signal strength, constrained to be non-negative, is fitted. The significance (σ) of the agreement between data and the Standard Model prediction is given, along with the model-independent 95% confidence level (CL) upper limit on the number of events ($N_{BSM}^{95\%}$) and cross-section times acceptance times efficiency ($\sigma_{BSM,max}^{95\%} \cdot A \cdot \epsilon$) from non-Standard-Model production. No significant deviations from the Standard Model prediction are found.

7 Interpretation

In the absence of significant discrepancies, exclusion limits at 95% CL are set in the context of several simplified supersymmetric models and a mSUGRA/CMSSM model, all described in Section 1. Theoretical uncertainties on the SUSY signals are estimated as described in Section 5.1. Combined experimental systematic uncertainties on the signal yield from jet energy scale, resolution, and pile-up are approximately $15 - 25\%$.

The limit for each signal region is obtained by comparing the observed event count with that expected from Standard Model background plus SUSY signal processes. All uncertainties on the Standard Model expectation, including those which are correlated between signal and background (for instance jet energy scale uncertainties) and all but theoretical cross section uncertainties (PDF and scale) on the signal expectation are taken into account. The resulting exclusion regions are obtained using the CL_s prescription [37]. For the multi-jet + flavour stream a simultaneous fit is performed in all the signal regions for each of the two values of p_T^{min}, and the two fit results are combined using the best expected limit per point in the parameter space, as described in Section 6.1. For the multi-jet + M_J^Σ stream the

signal region with the best expected limit at each point in parameter space is taken into account. The stream with the best expected limit at each point in parameter space is chosen when combining the two streams. The multi-jet + flavour stream typically has stronger expected exclusion limits compared to the multi-jet + M_J^Σ stream. However, in models with large number of objects in the final state, and more so in boosted topologies, the multi-jet + M_J^Σ stream becomes competitive.

As shown in what follows, the analysis substantially extends previous published exclusion limits on various models, from ATLAS [5, 6] and CMS [7, 38].

'Gluino-stop (off-shell)' model

An interpretation of the analysis result is done in a model that contains only a gluino octet and a neutralino $\tilde{\chi}_1^0$ within kinematic reach, and decaying with unit probability according to Eq. 2, via an off-shell $\tilde{t}$. The results are presented in the $m_{\tilde{g}} - m_{\tilde{\chi}_1^0}$ plane. Figure 8 shows the combined exclusion. Within the context of this simplified model, the 95% CL exclusion bound[5] on the gluino mass is 1.1 TeV for lightest neutralino masses up to 350 GeV.

'Gluino-stop (on-shell)' model

In this simplified model, each gluino of a pair decays as $\tilde{g} \rightarrow \tilde{t} + \bar{t}$; $\tilde{t} \rightarrow \tilde{\chi}_1^0 + t$. The mass of $\tilde{\chi}_1^0$ is fixed to 60 GeV. The results are presented in the $m_{\tilde{g}} - m_{\tilde{t}}$ plane. Figure 9 shows the combined exclusion limits; within the context of this simplified model, the 95% CL exclusion bound on the gluino mass is 1.15 TeV for stop masses up to 750 GeV.

'Gluino-squark (via $\tilde{\chi}_1^\pm$)' model

In this simplified model, each gluino of a pair decays as $\tilde{g} \rightarrow q + \tilde{q}$ and the squark as $\tilde{q} \rightarrow q + \tilde{\chi}_1^\pm \rightarrow q + W + \tilde{\chi}_1^0$. Two versions of this model are evaluated. In the first one, the fractional mass splitting, x, defined as $x = \frac{m_{\tilde{\chi}_1^\pm} - m_{\tilde{\chi}_1^0}}{m_{\tilde{g}} - m_{\tilde{\chi}_1^0}}$, is set to 1/2, and the $\tilde{\chi}_1^0$ mass varies. The results are presented in the $m_{\tilde{g}} - m_{\tilde{\chi}_1^0}$ plane. In the second, the $\tilde{\chi}_1^0$ mass is fixed to 60 GeV and x varies. In this case, the results are presented in the $m_{\tilde{g}} - x$ plane.

Figure 10 shows the combined exclusion limits in the two versions of this model. Gluino masses are excluded below 1 TeV at 95% CL, for $\tilde{\chi}_1^0$ masses below 200 GeV, in the case of x=1/2.

'Gluino-squark (via $\tilde{\chi}_1^\pm$ and $\tilde{\chi}_2^0$)' model

In this simplified model, each gluino of a pair decays as $\tilde{g} \rightarrow q + \tilde{q}$ and the squark as $\tilde{q} \rightarrow q + \tilde{\chi}_1^\pm \rightarrow q + W + \tilde{\chi}_2^0 \rightarrow q + W + Z + \tilde{\chi}_1^0$. The intermediate particle masses, $m_{\tilde{\chi}_1^\pm}$ and $m_{\tilde{\chi}_2^0}$, are set to $(m_{\tilde{g}} + m_{\tilde{\chi}_1^0})/2$ and $(m_{\tilde{\chi}_1^\pm} + m_{\tilde{\chi}_1^0})/2$ respectively. The results are presented in the $m_{\tilde{g}} - m_{\tilde{\chi}_1^0}$ plane. Figure 11 shows the combined exclusion limits for this model. Gluino masses are excluded below 1.1 TeV at 95% CL, for $\tilde{\chi}_1^0$ masses below 300 GeV.

mSUGRA/CMSSM

A mSUGRA/CMSSM model with parameters $\tan\beta = 30$, $A_0 = -2m_0$ and $\mu > 0$ is also used to interpret the analysis results. The exclusion limits are presented in the $m_0 - m_{1/2}$ plane. Figure 12 shows the

[5] Limits on sparticle masses quoted in the text are those from the lower edge of the $1\,\sigma$ signal cross section band rather than the central value of the observed limit, so can be considered conservative.

exclusion limits in this model, where, for large universal scalar mass m_0, gluino masses smaller than 1.1 TeV are excluded at 95% CL.

8 Conclusion

A search is presented for new phenomena with large jet multiplicities and missing transverse momentum using 20.3 fb^{-1} of 8 TeV pp collision data. The Standard Model predictions are found to be consistent with the data in signal regions of high jet multiplicity (from ≥ 7 to ≥ 10) plus missing transverse momentum. The sensitivity to new physics is enhanced by considering the number of b-tagged jets and the scalar sum of masses of radius $R = 1.0$ jets in the event. The results are interpreted in the context of a mSUGRA/CMSSM model that accomodates a lightest Higgs boson mass around the observed Higgs boson mass at the LHC, and various simplified models resulting to a final state with large jet multiplicity and $E_{\mathrm{T}}^{\mathrm{miss}}$. The exclusion limits substantially extend previous results. In a model where both of the pair-produced gluinos decay via $\tilde{g} \rightarrow t + \bar{t} + \tilde{\chi}_1^0$, gluino masses smaller than 1.1 TeV for neutralino masses below 350 GeV are excluded.

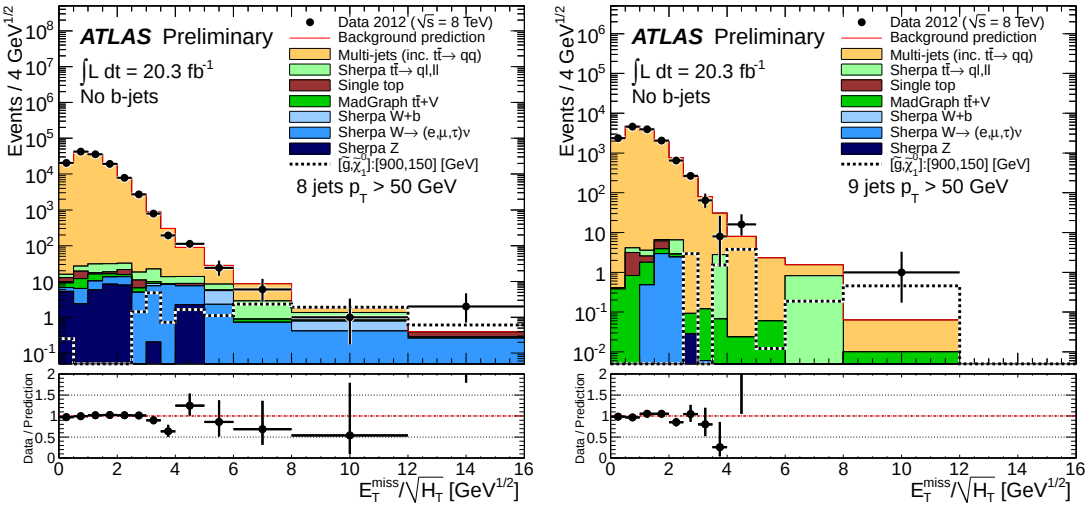

(a) 8j50, no b-jets (b) 9j50, no b-jets

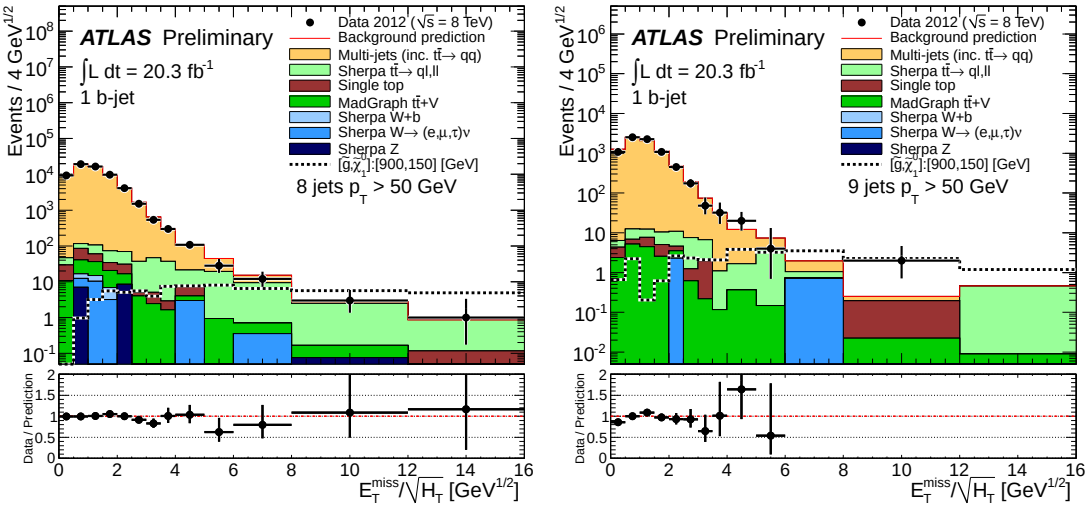

(c) 8j50, exactly one b-jet (d) 9j50, exactly one b-jet

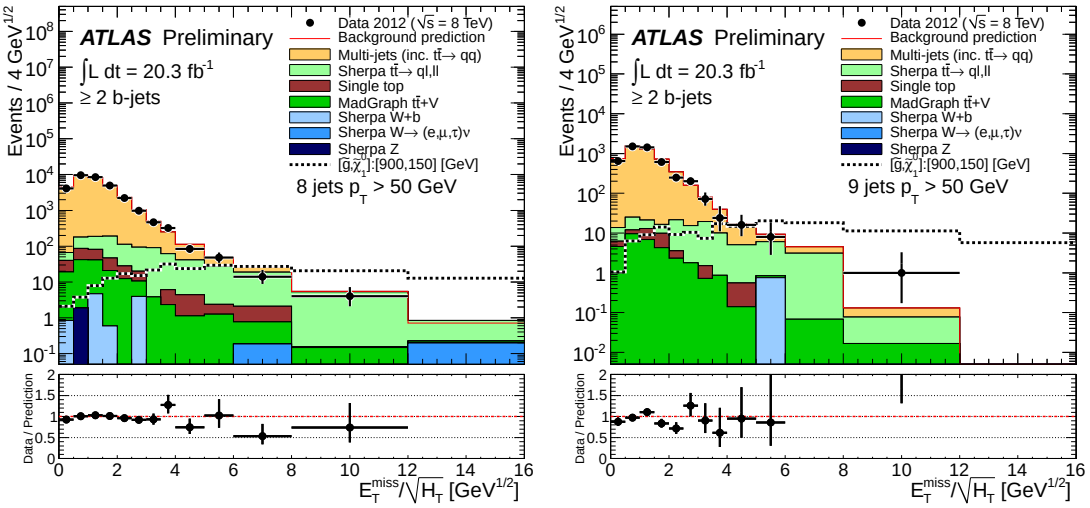

(e) 8j50, ≥ 2 b-jets (f) 9j50, ≥ 2 b-jets

Figure 5: $E_{\mathrm{T}}^{\mathrm{miss}}/\sqrt{H_{\mathrm{T}}}$ distributions for the multi-jet + flavour stream with $p_{\mathrm{T}}^{\mathrm{min}} = 50\,\mathrm{GeV}$, and either exactly eight jets (left) or exactly nine jets (right) with the signal region selection, other than that on $E_{\mathrm{T}}^{\mathrm{miss}}/\sqrt{H_{\mathrm{T}}}$ itself. The b-jet multiplicity increases from no b-jets (top) to exactly one b-jet (middle) to at least two b-jets (bottom). Other details as for Fig. 1.

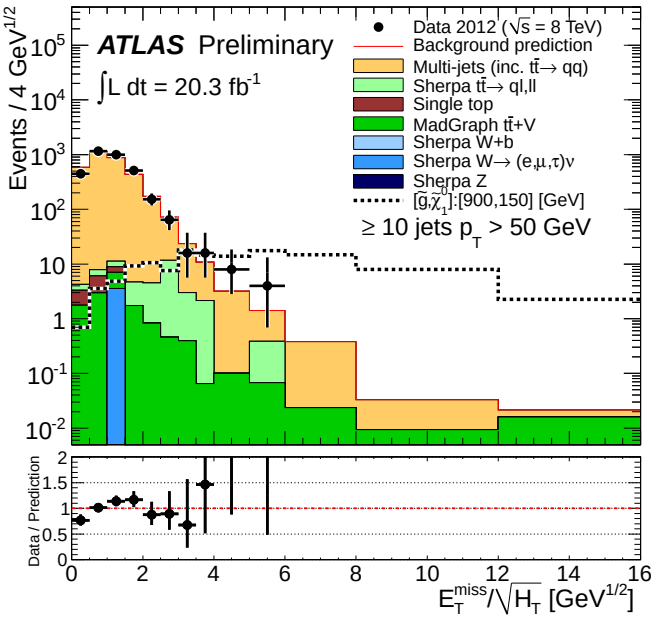

Figure 6: $E_{\mathrm{T}}^{\mathrm{miss}}/\sqrt{H_{\mathrm{T}}}$ distribution for the multi-jet + flavour stream with $p_{\mathrm{T}}^{\mathrm{min}} = 50\,\mathrm{GeV}$, and at least ten jets. The complete ≥ 10j50 selection has been applied, other than the final $E_{\mathrm{T}}^{\mathrm{miss}}/\sqrt{H_{\mathrm{T}}}$ requirement. Other details as for Fig. 1.

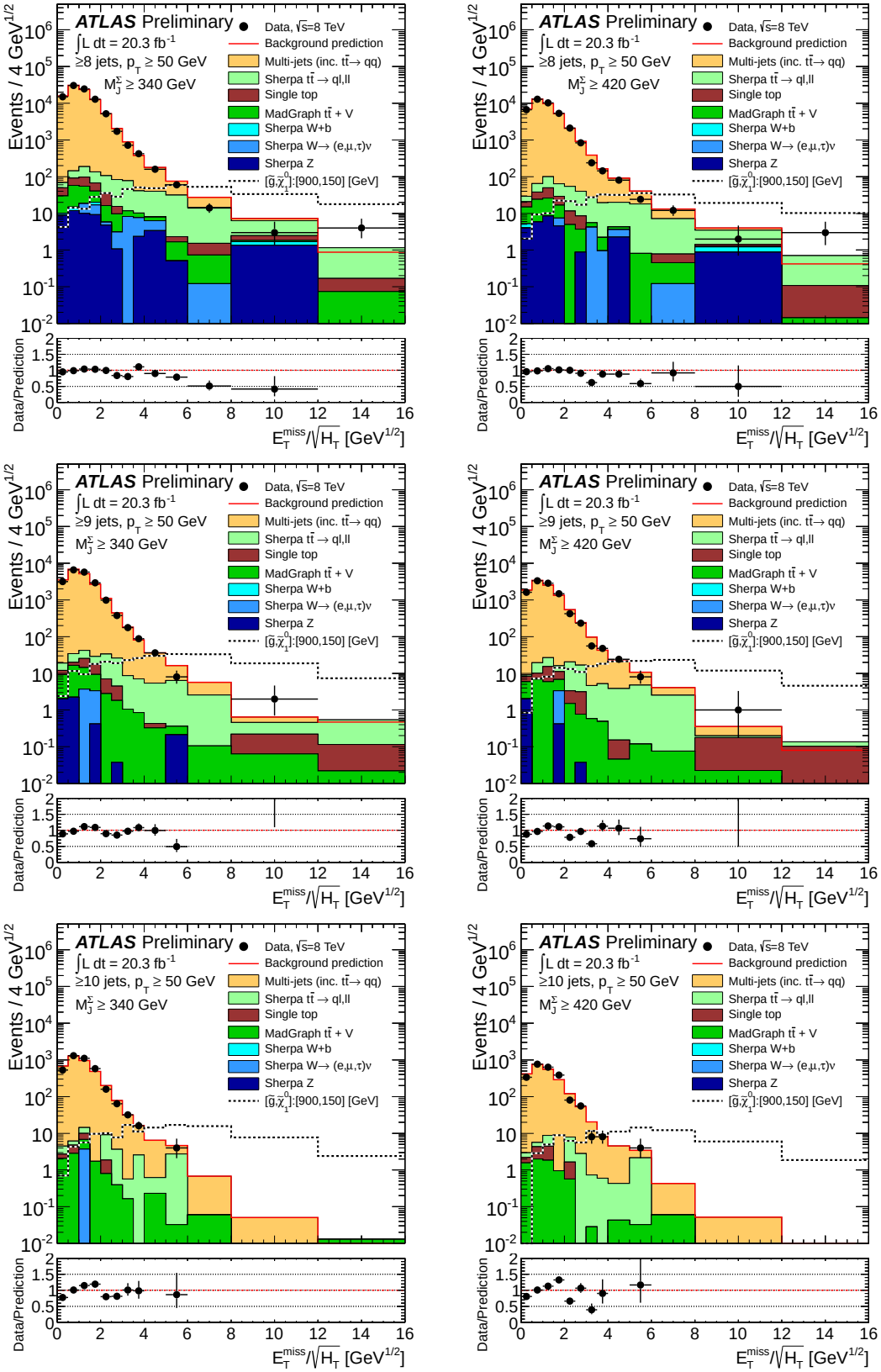

Figure 7: $E_{\mathrm{T}}^{\mathrm{miss}}/\sqrt{H_{\mathrm{T}}}$ distributions for the multi-jet + M_J^{Σ} stream with the signal region selection, other than the final $E_{\mathrm{T}}^{\mathrm{miss}}/\sqrt{H_{\mathrm{T}}}$ requirement. The figures on the left are for events with $M_J^{\Sigma} > 340\,\mathrm{GeV}$, while those on the right are for $M_J^{\Sigma} > 420\,\mathrm{GeV}$. The minimum multiplicity requirement for $p_{\mathrm{T}}^{\mathrm{min}} = 50$ GeV, $R = 0.4$ jets increases from eight (top) to nine (middle) and finally to ten jets (bottom). Other details as for Fig. 1.

Signal region	**8j50**			**9j50**			**10j50**
b-jets	0	1	≥ 2	0	1	≥ 2	—
Observed events	40	44	44	5	8	7	3
Total events after fit	35 ± 4	40 ± 10	50 ± 10	3.3 ± 0.7	6.1 ± 1.7	8.0 ± 2.7	1.37 ± 0.35
Fitted $t\bar{t}$	2.7 ± 0.9	11.8 ± 3.0	23.0 ± 5.0	0.36 ± 0.18	1.5 ± 0.5	3.2 ± 1.1	$0.06^{+0.09}_{-0.06}$
Fitted W+jets	$2.0^{+2.6}_{-2.0}$	$0.62^{+0.81}_{-0.62}$	$0.20^{+0.28}_{-0.20}$	-	$0.24^{+0.65}_{-0.24}$	-	-
Fitted others	$2.9^{+1.8}_{-1.8}$	$1.7^{+1.5}_{-1.2}$	$2.8^{+2.3}_{-2.0}$	0.03 ± 0.03	0.38 ± 0.25	$0.40^{+0.60}_{-0.24}$	0.08 ± 0.08
Total events before fit	36	48	59	3.4	6.6	8.9	1.39
$t\bar{t}$ before fit	3.5	15	30	0.41	1.8	4	0.08
W+jets before fit	2.9	1.0	0.29	-	0.40	-	-
Others before fit	2.4	1.8	2.8	0.03	0.34	0.4	0.08
Multi-jets	27 ± 3	30 ± 10	26 ± 10	3.0 ± 0.6	4.0 ± 1.4	4.4 ± 2.2	1.23 ± 0.32
$N^{95\%}_{BSM}$ (exp)	16	23	26	5	7	8	4
$N^{95\%}_{BSM}$ (obs)	20	23	22	7	9	7	6
$\sigma^{95\%}_{BSM,max} \cdot A \cdot \epsilon$ (exp) [fb]	0.8	1.2	1.3	0.26	0.36	0.40	0.19
$\sigma^{95\%}_{BSM,max} \cdot A \cdot \epsilon$ (obs) [fb]	0.97	1.1	1.1	0.34	0.43	0.37	0.29
p_0	0.24	0.5	0.7	0.21	0.28	0.6	0.13
Significance (σ)	0.7	-0.02	-0.6	0.8	0.6	-0.28	1.14

Table 4: Number of observed and expected (fitted) events for the seven $p_{\mathrm{T}}^{\mathrm{min}} = 50$ GeV signal regions of the flavour-tagged stream. The category indicated 'others' includes the contributions from $Z+$jets, $t\bar{t}+W$, $t\bar{t}+Z$, and single top.

Signal region	**7j80**			**8j80**		
b-jets	0	1	≥ 2	0	1	≥ 2
Observed events	12	17	13	2	1	3
Total fitted events	11.0 ± 2.2	17 ± 6	25 ± 10	0.9 ± 0.6	1.5 ± 0.9	3.3 ± 2.2
Fitted $t\bar{t}$	$0.00^{+0.26}_{-0.00}$	5.0 ± 4.0	12 ± 9	$0.10^{+0.14}_{-0.10}$	$0.32^{+0.67}_{-0.32}$	$1.5^{+1.9}_{-1.5}$
Fitted W+jets	$0.07^{+0.38}_{-0.07}$	$0.29^{+0.37}_{-0.29}$	-	-	-	-
Fitted others	$1.9^{+1.1}_{-0.9}$	$0.71^{+0.31}_{-0.25}$	$2.6^{+1.7}_{-1.1}$	0.02 ± 0.02	0.02 ± 0.02	$0.32^{+0.36}_{-0.21}$
Total events before fit	11.7	16	23	0.8	1.8	3.3
$t\bar{t}$ before fit	0.34	4	10	0.08	0.6	1.5
W+jets before fit	0.46	0.29	-	-	-	-
Others before fit	1.8	0.89	3.0	0.02	0.02	0.35
Multi-jets	9.1 ± 1.6	11 ± 4	10 ± 4	0.75 ± 0.56	1.2 ± 0.5	1.4 ± 1.0
N^{95}_{BSM} (exp)	10	17	14	4	4	6
N^{95}_{BSM} (obs)	10	16	12	5	3.5	6
$\sigma^{95\%}_{BSM,max} \cdot A \cdot \epsilon$ (exp) [fb]	0.5	0.8	0.7	0.18	0.18	0.31
$\sigma^{95\%}_{BSM,max} \cdot A \cdot \epsilon$ (obs) [fb]	0.5	0.8	0.6	0.24	0.17	0.31
p_0	0.5	0.6	0.8	0.19	0.6	0.5
Significance (σ)	0.05	-0.14	-1.0	0.9	-0.28	-0.06

Table 5: As for Table 4 but for the six signal regions for which $p_{\mathrm{T}}^{\mathrm{min}} = 80$ GeV.

Signal region	**8j50**	
M_J^{Σ} [GeV]	340	420
Observed events	69	37
Total events after fit	75 ± 19	45 ± 14
Fitted $t\bar{t}$	17 ± 11	16 ± 13
Fitted W+jets	$0.8^{+1.3}_{-0.8}$	$0.4^{+0.7}_{-0.4}$
Fitted others	$5.2^{+4.0}_{-2.5}$	$2.8^{+2.9}_{-1.6}$
Total events before fit	85	44
$t\bar{t}$ before fit	27	14
W+jets before fit	0.8	0.4
Others before fit	5	2.8
Multi-jets	52 ± 15	27 ± 7
$N^{95\%}_{BSM}$ (exp)	40	23
$N^{95\%}_{BSM}$ (obs)	35	20
$\sigma^{95\%}_{BSM,max} \cdot A \cdot \epsilon$ (exp) [fb]	1.9	1.1
$\sigma^{95\%}_{BSM,max} \cdot A \cdot \epsilon$ (obs) [fb]	1.7	1.0
p_0	0.60	0.7
Significance (σ)	-0.27	-0.6

Table 6: As for Table 4 but for the signal regions in the M_J^{Σ} stream for which the number of events in the control regions allowed for background determination using a fit.

Signal region	**9j50**		**10j50**	
M_J^Σ [GeV]	340	420	340	420
Observed events	13	9	1	1
Total events	17 ± 7	11 ± 5	$3.2^{+3.7}_{-3.2}$	2.2 ± 2.0
$t\bar{t}$	5 ± 4	$3.4^{+3.6}_{-3.4}$	$0.8^{+0.8}_{-0.8}$	$0.6^{+0.9}_{-0.6}$
W+jets	-	-	-	-
Others	$0.58^{+0.54}_{-0.33}$	$0.39^{+0.32}_{-0.30}$	0.12 ± 0.12	0.06 ± 0.06
Multi-jets	12 ± 4	7.0 ± 2.3	$2.3^{+3.6}_{-2.3}$	$1.6^{+1.8}_{-1.6}$
$N^{95\%}_{BSM}$ (exp)	13	11	5	5
$N^{95\%}_{BSM}$ (obs)	11	10	4	4
$\sigma^{95\%}_{BSM,max} \cdot A \cdot \epsilon$ (exp) [fb]	0.7	0.5	0.23	0.23
$\sigma^{95\%}_{BSM,max} \cdot A \cdot \epsilon$ (obs) [fb]	0.5	0.5	0.2	0.2
p_0	0.7	0.6	0.8	0.7
Significance (σ)	-0.6	-0.34	-0.8	-0.6

Table 7: As for Table 4 but for the signal regions in the M_J^Σ stream for which the number of events in the control regions did not allow for background determination using a fit and therefore the leptonic background is extracted directly from Monte Carlo simulations.

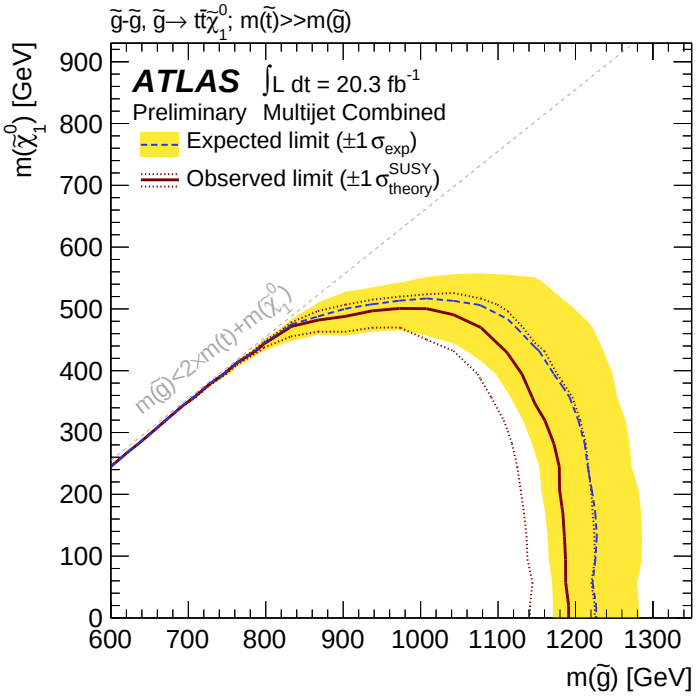

(a) Combined exclusion limit

Figure 8: 95% CL exclusion curve for the simplified gluino-stop (off-shell) model. The dashed grey and solid red lines show the 95% CL expected and observed limits, respectively, including all uncertainties except the theoretical signal cross section uncertainty (PDF and scale). The shaded yellow band around the expected limit shows the $\pm 1\sigma$ result. The $\pm 1\sigma$ lines around the observed limit represent the result produced when moving the signal cross section by $\pm 1\sigma$ (as defined by the PDF and scale uncertainties). The diagonal dashed line is the kinematic limit for this decay channel.

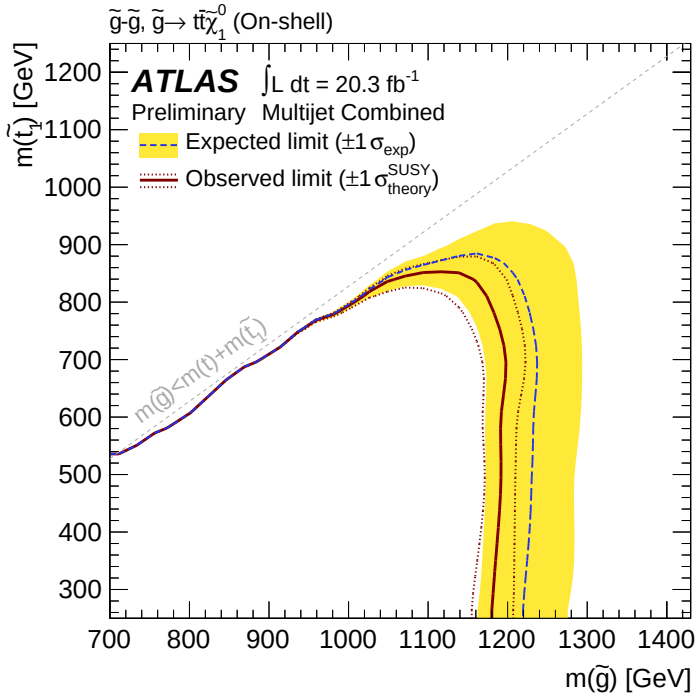

Figure 9: 95% CL exclusion curve for the simplified gluino-stop (on-shell) model, where the gluino decays as $\tilde{g} \rightarrow \tilde{t} + \bar{t}$ and the stop as $\tilde{t} \rightarrow \tilde{\chi}_1^0 + t$, with $m_{\tilde{\chi}_1^0} = 60$ GeV. Other details as in Fig. 8.

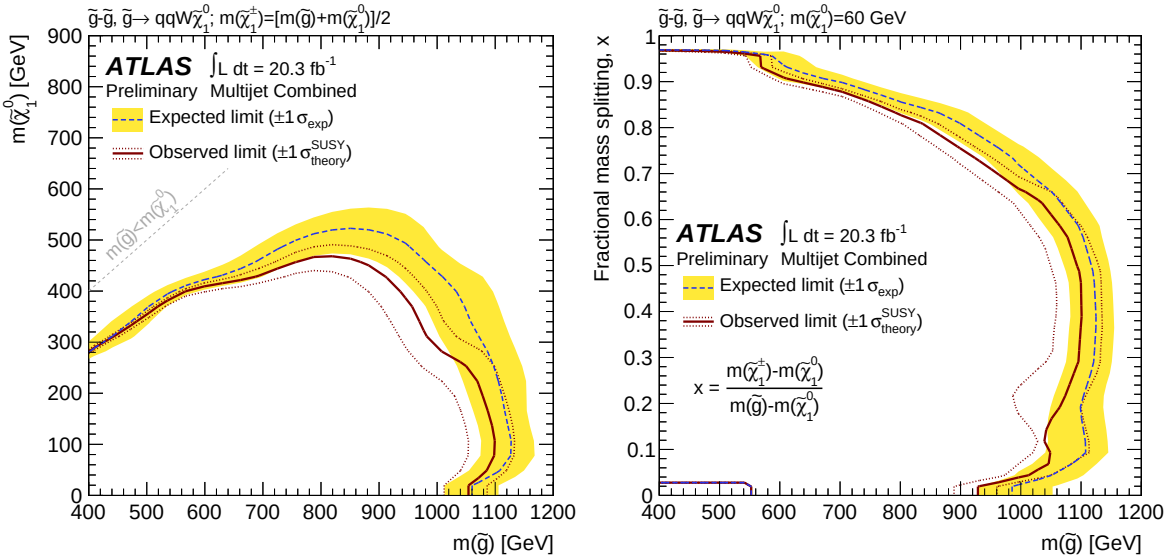

(a) x=1/2

(b) $m_{\tilde{\chi}_1^0} = 60$ GeV

Figure 10: 95% CL exclusion curve for the simplified gluino-squark (via $\tilde{\chi}_1^{\pm}$) model, for the two versions on the model; fixed x=1/2, where $x = \frac{m_{\tilde{\chi}_1^{\pm}} - m_{\tilde{\chi}_1^0}}{m_{\tilde{g}} - m_{\tilde{\chi}_1^0}}$, and varying $\tilde{\chi}_1^0$ mass on the left, and fixed $\tilde{\chi}_1^0$ mass to 60 GeV and varying x on the right. Other details as in Fig. 8.

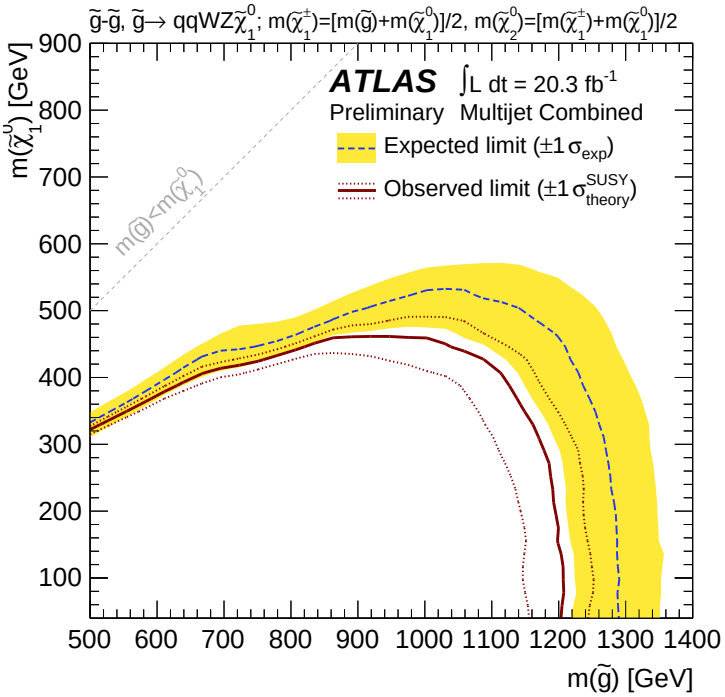

Figure 11: 95% CL exclusion curve for the simplified gluino-squark (via $\tilde{\chi}_1^\pm$ and $\tilde{\chi}_2^0$) model. Other details as in Fig. 8.

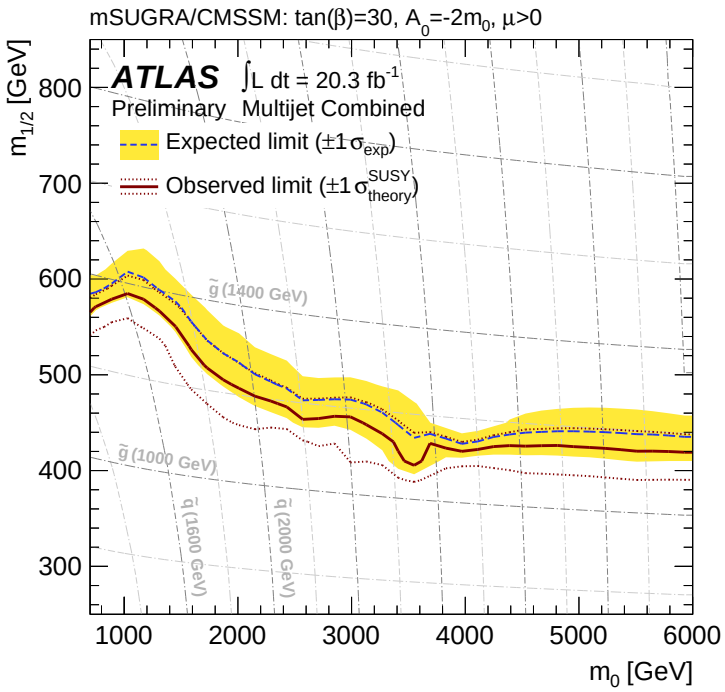

Figure 12: 95% CL exclusion curve for the mSUGRA/CMSSM model, generated with parameters $\tan\beta = 30$, $A_0 = -2m_0$ and $\mu > 0$. Other details as in Fig. 8.

References

[1] L. Evans, (ed.) and P. Bryant, (ed.), JINST **3** (2008) S08001.

[2] P. Fayet, Phys.Lett. **B64** (1976) 159.

P. Fayet, Phys.Lett. **B69** (1977) 489.

G. R. Farrar and P. Fayet, Phys.Lett. **B76** (1978) 575.

P. Fayet, Phys.Lett. **B84** (1979) 416.

S. Dimopoulos and H. Georgi, Nucl.Phys. **B193** (1981) 150.

[3] H. Goldberg, Phys.Rev.Lett. **50** (1983) 1419.

J. R. Ellis, J. Hagelin, D. V. Nanopoulos, K. A. Olive, and M. Srednicki, Nucl.Phys. **B238** (1984) 453.

[4] ATLAS Collaboration, JHEP **11** (2011) 099, arXiv:1110.2299 [hep-ex].

[5] ATLAS Collaboration, JHEP **1207** (2012) 167, arXiv:1206.1760 [hep-ex].

[6] ATLAS Collaboration, Eur.Phys.J. **C72** (2012) 2174, arXiv:1207.4686 [hep-ex].

[7] CMS Collaboration, arXiv:1303.2985 [hep-ex]. Submitted to EPJC.

[8] CMS Collaboration, arXiv:1212.6961 [hep-ex]. Submitted to Phys. Rev. Lett.

[9] CMS Collaboration, Phys.Rev.Lett. **109** (2012) 171803, arXiv:1207.1898 [hep-ex].

[10] A. H. Chamseddine, R. L. Arnowitt, and P. Nath, Phys.Rev.Lett. **49** (1982) 970.

R. Barbieri, S. Ferrara, and C. A. Savoy, Phys. Lett. **B119** (1982) 343.

L. E. Ibanez, Phys.Lett. **B118** (1982) 73.

L. J. Hall, J. D. Lykken, and S. Weinberg, Phys.Rev. **D27** (1983) 2359.

N. Ohta, Prog.Theor.Phys. **70** (1983) 542.

G. L. Kane, C. F. Kolda, L. Roszkowski, and J. D. Wells, Phys.Rev. **D49** (1994) 6173, arXiv:hep-ph/9312272.

[11] M. Cacciari, G. P. Salam, and G. Soyez, JHEP **04** (2008) 063, arXiv:0802.1189.

M. Cacciari and G. P. Salam, Phys. Lett. **B641** (2006) 57, arXiv:hep-ph/0512210.

[12] A. Hook, E. Izaguirre, M. Lisanti, and J. G. Wacker, Phys.Rev. **D85** (2012) 055029, arXiv:1202.0558 [hep-ph].

[13] ATLAS Collaboration, Phys.Lett. **B716** (2012) 1, arXiv:1207.7214 [hep-ex].

CMS Collaboration, Phys.Lett. **B716** (2012) 30, arXiv:1207.7235 [hep-ex].

[14] ATLAS Collaboration, arXiv:1302.4393 [hep-ex].

[15] C. Issever, K. Borras, and D. Wegener, Nucl.Instrum.Meth. **A545** (2005) 803, arXiv:physics/0408129 [physics].

ATLAS Collaboration, arXiv:1112.6426 [hep-ex].

[16] M. Cacciari and G. P. Salam, Phys.Lett. **B659** (2008) 119, arXiv:0707.1378 [hep-ph].

[17] ATLAS Collaboration,. ATLAS-CONF-2011-102.

[18] ATLAS Collaboration,. ATLAS-CONF-2012-097.

[19] ATLAS Collaboration, Eur.Phys.J. **C72** (2012) 1909, arXiv:1110.3174 [hep-ex].

[20] ATLAS Collaboration, Eur.Phys.J. **C72** (2012) 1844, arXiv:1108.5602 [hep-ex].

[21] T. Gleisberg et al., JHEP **02** (2009) 007, arXiv:0811.4622.

[22] H.-L. Lai, M. Guzzi, J. Huston, Z. Li, P. M. Nadolsky, et al., Phys.Rev. **D82** (2010) 074024, arXiv:1007.2241 [hep-ph].

[23] M. Aliev, H. Lacker, U. Langenfeld, S. Moch, P. Uwer, et al., Comput. Phys. Commun. **182** (2011) 1034, arXiv:1007.1327 [hep-ph].

S. Catani, L. Cieri, G. Ferrera, D. de Florian, and M. Grazzini, Phys.Rev.Lett. **103** (2009) 082001, arXiv:0903.2120 [hep-ph].

[24] S. Frixione and B. R. Webber, JHEP **06** (2002) 029, arXiv:hep-ph/0204244.

S. Frixione, F. Stoeckli, P. Torrielli, B. R. Webber, and C. D. White, arXiv:1010.0819 [hep-ph].

S. Frixione, E. Laenen, P. Motylinski, and B. R. Webber, JHEP **0603** (2006) 092, arXiv:hep-ph/0512250 [hep-ph].

S. Frixione, E. Laenen, P. Motylinski, B. R. Webber, and C. D. White, JHEP **0807** (2008) 029, arXiv:0805.3067 [hep-ph].

[25] G. Corcella, I. Knowles, G. Marchesini, S. Moretti, K. Odagiri, et al., arXiv:hep-ph/0210213 [hep-ph].

[26] J. M. Butterworth, J. R. Forshaw, and M. H. Seymour, Z. Phys. **C72** (1996) 637, arXiv:hep-ph/9601371.

[27] B. P. Kersevan and E. Richter-Was, arXiv:hep-ph/0405247v3 [hep-ph].

[28] T. Sjöstrand, S. Mrenna, and P. Z. Skands, JHEP **05** (2006) 026, arXiv:hep-ph/0603175.

[29] J. Alwall, M. Herquet, F. Maltoni, O. Mattelaer, and T. Stelzer, JHEP **1106** (2011) 128, arXiv:1106.0522 [hep-ph].

[30] M. Bähr et al., Eur. Phys. J. **C58** (2008) 639, arXiv:0803.0883.

[31] J. Pumplin et al., JHEP **07** (2002) 012, arXiv:hep-ph/0201195.

[32] W. Beenakker, R. Hopker, M. Spira, and P. M. Zerwas, Nucl. Phys. **B492** (1997) 51, arXiv:hep-ph/9610490.

A. Kulesza and L. Motyka, Phys.Rev.Lett. **102** (2009) 111802, arXiv:0807.2405 [hep-ph].

A. Kulesza and L. Motyka, Phys.Rev. **D80** (2009) 095004, arXiv:0905.4749 [hep-ph].

W. Beenakker, S. Brensing, M. Kramer, A. Kulesza, E. Laenen, et al., JHEP **0912** (2009) 041, arXiv:0909.4418 [hep-ph].

W. Beenakker, S. Brensing, M. Kramer, A. Kulesza, E. Laenen, et al., Int.J.Mod.Phys. **A26** (2011) 2637, arXiv:1105.1110 [hep-ph].

[33] M. Kramer, A. Kulesza, R. van der Leeuw, M. Mangano, S. Padhi, et al., arXiv:1206.2892 [hep-ph].

[34] ATLAS Collaboration, Eur. Phys. J. **C70** (2010) 823, arXiv:1005.4568 [physics.ins-det].

[35] GEANT4 Collaboration, S. Agostinelli et al., Nucl. Instrum. Meth. **A506** (2003) 250.

[36] M. L. Mangano, M. Moretti, F. Piccinini, R. Pittau, and A. D. Polosa, JHEP **07** (2003) 001, arXiv:hep-ph/0206293.

[37] A. Read, Journal of Physics G: Nucl. Part. Phys. **28** (2002) 2693.

[38] CMS Collaboration, arXiv:1301.2175 [hep-ex].